Published in final edited form as:

Biosens Bioelectron. 2020 October 01; 165: 112221. doi:10.1016/j.bios.2020.112221.

Measuring Glucose at the Site of Insulin Delivery with a Redox-Mediated Sensor

Peter G. Jacobs[1], **Nichole Tyler**[1], **Scott M. Vanderwerf**[2], **Clara Mosquera-Lopez**[1], **Thomas Seidl**[2], **Robert Cargill**[2], **Deborah Branigan**[3], **Katrina Ramsey**[4], **Kristin Morris**[2], **Sheila Benware**[2], **W. Kenneth Ward**[2], **Jessica Castle**[3]

[1]Artificial Intelligence for Medical Systems (AIMS) Lab, Oregon Health & Science University, 3303 SW Bond Ave., Portland OR 97232

[2]Pacific Diabetes Technologies, 12172 SW Garden Pl, Portland, Oregon OR 97223

[3]Harold Schnitzer Diabetes Health Center, Oregon Health & Science University, 3147 SW Sam Jackson Park, Portland OR 97239

[4]OHSU Department of Biostatistics, Oregon Health & Science University, 3147 SW Sam Jackson Park, Portland OR 97239

Abstract

Automated insulin delivery systems for people with type 1 diabetes rely on an accurate subcutaneous glucose sensor and an infusion cannula that delivers insulin in response to measured glucose. Integrating the sensor with the infusion cannula would provide substantial benefit by reducing the number of devices inserted into subcutaneous tissue. We describe the sensor chemistry and a calibration algorithm to minimize impact of insulin delivery artifacts in a new glucose sensing cannula. Seven people with type 1 diabetes undergoing automated insulin delivery used two sensing cannulae whereby one delivered a rapidly-acting insulin analog and the other delivered a control phosphate buffered saline (PBS) solution with no insulin. While there was a small artifact in both conditions that increased for larger volumes, there was no difference between the artifacts in the sensing cannula delivering insulin compared with the sensing cannula delivering PBS as determined by integrating the area-under-the-curve of the sensor values following delivery of larger amounts of fluid ($P=0.7$). The time for the sensor to recover from the artifact was found to be longer for larger fluid amounts compared with smaller fluid amounts (10.3 ± 8.5 minutes vs. 41.2 ± 78.3 seconds, $P<0.05$). Using a smart-sampling Kalman filtering smoothing algorithm improved sensor accuracy. When using an all-point calibration on all sensors, the smart-sampling Kalman filter reduced the mean absolute relative difference from 10.9% to 9.5% and resulted in 96.7% of the data points falling within the A and B regions of the Clarke error grid. Despite a small artifact, which is likely due to dilution by fluid delivery, it is possible to continuously measure glucose in a cannula that simultaneously delivers insulin.

Corresponding author: Peter G. Jacobs, 503-358-2291, www.ohsu.edu/jacobs.

Peter G. Jacobs: Writing Original Draft, Conceptualization, Methodology, Investigation, Project Administration, Supervision, Writing – Review & Editing, Funding Acquisition, Supervision, Data Curation, Formal analysis. W. Kenneth Ward, Robert Cargill, Thomas Seidl, Jessica Castle: Conceptualization, Methodology, Investigation, Project Administration, Supervision, Writing – Review & Editing, Funding Acquisition, Supervision. Scott M. Vanderwerf: Conceptualization, Methodology, Writing-Review & Editing, Investigation, Project Management. Nichole Tyler, Clara Mosquera-Lopez, Katrina Ramsey: Formal analysis, Data Curation, Writing-Review & Editing, Visualization. Kristin Morris, Sheila Benware: Investigation, Software.

Keywords

continuous glucose monitoring; redox-mediated electrochemistry; amperometric sensor; insulin infusion

Introduction

Automated insulin delivery (AID) systems have become commercially available in recent years and systems like the Medtronic 670G (Smalley 2016) are now being used by thousands of people with type 1 diabetes (T1D) worldwide. AID systems have been shown to improve glycemic outcomes in people with T1D (Kropff et al. 2015; Russell et al. 2014; Thabit et al. 2014; Weisman et al. 2017), especially during the night (Hovorka et al. 2011; Peters and Haidar 2018; Renard et al. 2016). Recently, our group has shown how AID systems along with automated glucagon delivery can help prevent hypoglycemia during exercise (Castle et al. 2018; Jacobs et al. 2016). AID systems typically require subcutaneous insertion of a continuous glucose monitor (CGM) to measure interstitial glucose. AID systems also require insertion of an insulin infusion cannula to deliver insulin in response to the sensed glucose. The complexity of requiring two devices, a sensor and a cannula, to be inserted into two separate locations in the body can be a major reason why potential users of the system fail to adopt the technology. In addition, device insertion may cause skin reactions including scarring. For these reasons and others, less than 12% of people with T1D currently use an insulin pump and CGM concurrently (Foster et al. 2016), although this number may be higher as both CGM and insulin pump usage has increased in recent years (Foster et al. 2019).

One reason why glucose sensors and insulin delivery cannulae have not been integrated into AID systems is because excipients in the insulin formulation, including *m*-cresol and phenol, have been shown to cause several types of artifact in conventional (peroxide-measuring) sensors. The marked initial rise in current can be mistaken for hyperglycemia, and we previously described a longer-term loss of sensitivity due to electropolymerization of an insulator onto the sensor electrode (Ward et al. 2017). This initial rise in current followed by a loss of sensitivity was shown to be present in peroxide-sensing devices and was likely due to phenol and m-cresol excipients present in all current insulin formulations. As is discussed further below, the effect could be mitigated by instead using an osmium-ligand-based layer that enables a lower bias potential on the electrode. Other groups have also researched these types of artifacts and measurement of glucose at the site of insulin delivery has been studied by a number of these groups. Lindpointner et al (2010), using a microdialysis system, found that the physiologic effect of insulin delivery to decrease local glucose concentration was actually quite minimal. Later, this same group further showed that continuously delivering insulin while extracting interstitial fluid from the infusion site, the glucose measured at the site of insulin delivery was not significantly different than plasma glucose levels (Regittnig et al. 2013). Rodriguez et al. (2011) placed sensors 0.5, 1, 2, and 3 cm (“near sensors”) and 10–15 cm (“far sensors”) from the insulin injection site and investigated the timing and magnitude of the glucose decline following a single insulin injection. They did not find a statistically significant difference in the time the sensors detected a decline in glucose

for the near vs. the far sensors. They did find that there was a difference in how far the glucose fell for the 0.5 and 3 cm sensors relative to the far sensors. Hermanides et al. (2008) placed two microdialysis sensors close to the point of insulin infusion, one at 0.9 cm and one at 10 cm, and found that there was no difference in the sensor readings between the sensors, but that there was a 5-minute delay in response time between the sensors. They were specifically interested in whether microdialysis CGM devices could be inserted near insulin infusion sites. Linde and Philip (1989) showed that injection of 0.25 ml of insulin leads to an average subcutaneous distribution radius of 7 mm, so the placement of the sensor beyond 7 mm from the infusion site may explain why there was no difference in the sensor measurements from the near and far sensors in Hermanides' work. O'Neal et al., (2013) evaluated a co-located peroxide-measuring sensor and insulin delivery cannula that were separated by 11 mm and found that accuracy of the co-located sensor was comparable with that of the sensor located far from the insulin site. However, this study ran for just over 48 hours, with frequent calibrations that may have obscured long-term effects of insulin interference. Although the sensor and cannula were near one another on the same platform, the sensor was not positioned directly on the cannula requiring two separate inserter needles compared to one in our design.

Nacht et al. (2015) showed that using an optical based glucose sensor that relies on near infrared and phosphorescent porphyrin dyes that may be measured using a fluorometer measurement module, glucose could be measured at the site of insulin delivery with minimal impact of insulin on sensor accuracy. However, there was still a large amount of error for this sensor, especially in the low and high ranges of sensor values where the negative impact on patients can be the most serious.

Our prior work in swine (Ward et al. 2017) has shown that, in a conventional peroxide-sensing device, phenol and *m*-cresol excipients present in all current insulin formulations can lead to sensor artifacts when the glucose is sensed at the same location as the insulin is delivered. These are characterized by a rapid, sustained increase in sensor current, followed by a gradual loss of sensitivity that ultimately renders the sensor unusable. However, when an osmium-ligand-based layer is immobilized on a gold electrode and poised at a low bias potential, such artifacts were absent. Osmium-based redox mediated glucose sensing systems are also used in the Freestyle product line of Abbott Laboratories.

In this paper we extend the work done previously in Ward et al. and show performance in humans of the glucose sensor with an osmium-based mediated chemistry polarized at a low bias potential mounted on a cannula that delivers insulin. We performed an in-clinic experiment in humans with T1D who used two glucose sensing cannulae during an 8-hour study period. One of the glucose sensing cannulae was delivering insulin based on a fading memory proportional-derivative control algorithm (Jacobs et al. 2014) while the second glucose sensing cannula was delivering an equivalent volume of phosphate-buffered saline (PBS) solution. Delivery amounts of insulin and PBS were categorized as either large *meal boluses* given at the time of meals which typically are greater than 0.83 units or *basal insulin* that is dosed in smaller amounts (<0.83 units) every 5 minutes to maintain glycemic levels throughout the day. In our study, all basal insulin deliveries were less than 0.83 units and all bolus insulin was greater than 0.83 units. We found that there is a small artifact when

delivering either small amounts of basal insulin or control PBS through a glucose-sensing cannula, but that the artifact is not caused by insulin *per se*. The artifact was found to be larger and required more time to recover for larger meal boluses compared with basal delivery amounts. Smart sampling and signal processing methods are shown that describe how the artifact can be mitigated.

Contributions

The specific contributions of this manuscript include the following. First, we have quantified the size and the duration of an artifact generated by delivering various amounts of fluid through a glucose-sensing cannula close to the sensing site. Second, we have demonstrated that the redox sensing chemistry described herein is sufficient to eliminate artifacts from insulin excipients such as m-cresol or phenol given that the artifact generated by delivery of insulin is identical to that caused by delivery of an equivalent amount of PBS. And finally, we provide new signal processing methods for mitigating the impact of the artifact, and to improve sensing accuracy.

Methods

Common terminology and metrics used in glucose sensing

This manuscript uses a number of well-established metrics to assess the accuracy of the glucose sensing cannula. The sensor accuracy is assessed using the mean absolute relative error (MARE) and the mean relative error (MRE), which are discussed further under the Calibration section in Equations 2 and 3. The MARE provides an estimate of the absolute error in measurement of glucose as a percentage relative to a reference glucose, which is typically measured through a blood sample using a Yellow Springs Instrument (YSI) machine by a skilled technician (Yellow Springs Instruments, Yellow Springs, OH). The MRE is also a percentage error relative to a YSI glucose value, but since it is not an absolute value, it provides information on whether there is a positive or negative bias on the measured glucose. Glucose accuracy is also assessed using a Clarke error grid (Clarke et al. 1987), which is a scatter plot of measured glucose vs. actual glucose, where the x-axis is the reference glucose which is again typically assessed using. The Clarke error grid provides regions that are clinically safe (A and B) and also regions that are progressively more dangerous (C, D, and E). The A and B regions of the Clarke error grid are generally considered safe, and they represents the diagonal region of the graph where the glucose sensor closely matches the reference glucose. The D and E regions represent regions where the glucose sensor is inaccurate in a zone where the measurement, if used by a patient, could cause harm if they act on the measurement. For example, the upper left E regions is where the reference glucose is low (e.g. <3.9 mmol/L) but the predicted glucose is high (e.g. > 10 mmol/L). If a patient acted on an inaccurate high sensor value in this case, they would inject additional insulin into their body, which could be fatal. Commercial glucose sensors typically have an MARE in the range of 7–10%, with over 90% of sensor glucose in the A and B regions, and 0% in the D and E regions of the Clarke error grid. In this paper, we use MARE, MRE, and the Clarke error grid to assess accuracy of the sensing cannula.

All implanted electrochemical sensing electrodes require a *run-in time*, which is the time required for the sensor to stabilize immediately after it is inserted into the body. A run-in time is typically required because immediately upon insertion of a sensor into a mammal, there are very rapid changes in current and for this reason, these early values are unstable. The current measured shortly after insertion is very high and it starts to fall within seconds in an exponential fashion. The initial spike may be due to oxidation of the gold surface of the indicating electrode such that as more and more of the gold surface becomes oxidized, and thus not available for continued oxidation, the current declines. In addition, there is a very rapid deposition of interstitial proteins over the outer sensor membrane, which partially blocks glucose entry and also contributes to the time-related lowering of the glucose-induced current. When these two processes are largely complete, the sensor current becomes stable. At this time, the “run-in” or “warm-up time” is complete. For the sensing cannula used in this analysis, a run-in time of 3.5 hours was used.

Sensing cannula design

The sensors used in this study (Figure 1) were similar to the design described in Ward et al. (2017). Prior to their separation into individual sensing units, sensors were fabricated into planar electrode arrays with 48 sensor units per array as described in Ward et al. Each sensor unit was comprised of a silver reference electrode and two gold indicating electrodes. A custom built sputter chamber was used to apply the metals to a titanium foil that had been laminated onto a flexible polyimide sheet. Patterns and shapes of the electrodes were created using photolithography techniques and microablation using an infrared wavelength (1064 nm) laser tool. The silver electrode was converted to a Ag/AgCl combined counter/reference electrode by exposing the silver to ferric chloride. The individual sensor units were separated from the array using an ultraviolet wavelength (355 nm) laser tool. The flexible individual sensor units were then laminated to the surface of a 25 gauge stainless steel tube using epoxy cement. The sensing cannula extended 12 mm into the tissue at a 40° angle; depth beneath skin was approximately 7–8 mm.

A skin-worn battery-powered electronic module (Supplemental Figure 4) was developed to (1) provide the bias potential to the sensor, (2) convert the current generated by the glucose sensor to a proportional voltage using a transimpedance amplifier, and (3) sample and transmit the glucose sensor data wirelessly to a laptop computer using a microcontroller and a Bluetooth Low Energy radio transceiver chip (NRF-51822; Nordic Inc). The current data (in nano-Amperes) was sampled every 2 seconds.

Sensing cannula electrochemistry

The chemistry of the redox-mediated sensor, as described in Ward et al.(2017), included osmium coordinated within a ligand, followed by binding the osmium/ligand complex to a polymer chain. As a redox mediator, osmium was used because it is suitable for accepting electrons from glucose oxidase, more specifically from the prosthetic group of glucose oxidase (flavin adenine dinucleotide, FAD). We elected to bind the osmium to the ligand 4,4′-dimethyl 2,2′-bipyridine because osmium coordinated to this ligand provided higher currents than two other ligands that we tested (bipyridine bound to two amino groups and bipyridine bound to two methoxy groups). After the osmium-ligand complex was formed,

this complex was bound to a polymer backbone, poly(N-vinyl imidazole, PVI) (BOC Sciences). Once the osmium ligand complex is bound to PVI, the entire complex is bound to a gold electrode poised at 175–180 mV vs Ag/AgCl reference electrode. The electrons originated from glucose are transported to the gold electrode on which the osmium-ligand-backbone is deposited, thus creating a glucose-induced current that is not adversely affected by excipients in commercial insulin formulations. As the electrons are donated to the gold electrode, the osmium mediator switches back to its oxidized state and can then acquire more electrons from the FAD group of the glucose oxidase when glucose is present. In Ward et al. (2017) we discuss how we found through cyclic voltammetry experiments that the maximal current of the sensor when exposed to glucose was at 175 mV. And at that voltage, there was no interference from phenol, meta-cresol, acetaminophen, ascorbic acid and uric acid. Therefore, there was no benefit of biasing at a lower voltage

Preparation of osmium-ligand complex and osmium-ligand-backbone complex

One molar part of K_2OsCl_6 is dissolved in ethylene glycol and 2.5–3 molar parts of 4,4’ dimethyl 2,2’ bipyridine are added. The solution is refluxed for 12–24 hours in a fume hood at atmospheric pressure and at a temperature of 200°C. In terms of the reflux apparatus procedure, the key substrates stay in the lower spherical part of the apparatus. In contrast, since the temperature is kept at or slightly above the boiling point of the solvent, some of the solvent evaporates into the vertical tubular element, then immediately condenses and returns to the lower part. Since the temperature of a boiling solution remains at the boiling point even when excess heat is applied, the use of the reflux condensing procedure is a convenient way to continuously keep a solution at a very specific temperature (based on the choice of solvent) for a prolonged period of time.

Safety note: Some forms of osmium are very toxic to mammals, and thus dermal or respiratory exposure must be avoided.

After evaporation of the ethylene glycol, the solid (osmium bound to the 4,4’ dimethyl 2,2’) is reacted with poly(N-vinyl imidazole, PVI) in the same way as described above, i.e. using reflux condensing held at 200°C in ethylene glycol for 12–24 hours. The molar ratios can be calculated using the average molecular weight of the particular batch of PVI and the fact that the desired ratio is one osmium-ligand complex per every 6–10 repeating vinyl imidazole units. The ethylene glycol is removed (evaporated), leaving the osmium-ligand-PVI complex as a solid brown material. This material is then mixed with glucose oxidase (Sigma-Aldrich) at a temperature of about 35–45°C, avoiding higher temperatures that could denature the glucose oxidase. This mixture, applied on a clean gold electrode, is then exposed to glutaraldehyde (Sigma-Aldrich) vapor in a fume hood for 1–2 hours (glutaraldehyde has a very high vapor pressure and is probably toxic, thus exposure to humans must be avoided). The glutaraldehyde crosslinks the glucose oxidase and thus avoids leaching of the enzyme into mammalian tissue (glucose oxidase is not a mammalian protein and probably can cause serious allergic reactions in mammals). The electrode, now coated with glucose oxidase and osmium-ligand-PVI backbone, is then coated with an outer membrane of polyurethane as follows: An outer membrane by dip coating into a solvated blend of polyvinylpyridine-co-styrene (PVP-co-S) with commercially available Pellethane and a silicone containing polyurethane. The polymer blend admixed in 1:1

dimethylacetamide (DMAc) and THF. Dip coating results in a coating deposited over the top of the glucose oxidase/osmium-ligand/polymer backbone. After the polyurethane-solvent solution is coated on to the glucose oxidase/osmium-ligand/polymer backbone, the solvent completely evaporates, leaving behind a pure film of polyurethane, coating the other layers.

Sensor signal processing using 2-stage Kalman smoother

The raw sensor current data was smoothed using a two-stage Kalman filter algorithm described in the Supplementary Materials.

Study design

In this study, we evaluated the accuracy of the glucose sensing cannula in people with T1D and quantified the measurement artifact caused by delivery of both insulin and PBS during automated delivery of insulin for maintaining glucose control in these study participants. The sensing cannula was not used to inform the AID system; rather a commercial G6 glucose sensor developed by Dexcom (San Diego, CA) was used to inform the AID of the participant's interstitial glucose throughout the day. For this study, we used a previously described AID (Jacobs et al. 2014; Jacobs et al. 2015) that runs on a smart phone and communicates wirelessly with both a continuous glucose monitor from Dexcom and a research grade insulin pump from Tandem (San Diego, CA). The protocol for this study is described at https://clinicaltrials.gov (NCT03528174).

Cohort

A total of eleven people with T1D were recruited for this study. Inclusion criteria included age 21–65 years, use of insulin pump for >3 months, glycated hemoglobin or HbA1c ≤ 86 mmol/mol (10%), using less than 200 units of insulin per day, and body mass index or BMI > 22. Exclusion criteria included pregnancy or intention of becoming pregnant, cardiovascular, liver or kidney disease, anemia, history of diabetic ketoacidosis within 6 months or severe hypoglycemia within 12 months. One participant was disqualified during screening, two participants had adhesive failures during the study yielding incomplete data, and one participant experienced severe nausea unrelated to the study that prevented them from completing the study leaving data from 7 participants for analysis.

Protocol

Participants arrived at the Oregon Health & Science University Oregon Clinical and Translational Research Institute at 7 AM. At 9 AM the two glucose sensing cannulae were inserted into the participant, one on either side of his/her abdomen. One of the sensing cannulae was connected to a Tandem t:slim TAP3 pump (Tandem, San Diego CA) and filled with aspart insulin (Novolog, Novo-Nordisk A/S) while the second sensing cannula was connected to a Tandem t:slim TAP3 pump filled with PBS control solution. Each participant also had a Dexcom G6 continuous glucose monitoring (CGM) sensor inserted into to their abdomen when they arrived at the clinic. The G6 CGM transmitted glucose data from the sensor to a Google Nexus phone via wireless Bluetooth low energy (BTLE). The Google Nexus smart phone was running the OHSU iPancreas app used in various other studies (Castle et al. 2018; Jacobs et al. 2014; Jacobs et al. 2016) that included a fading

memory proportional-derivative (FMPD) control algorithm for automating insulin based on the Dexcom CGM data. An FMPD algorithm calculates the amount of insulin to deliver to a person living with diabetes based off of their current glucose level and the rate of change of their glucose. The proportional part of an FMPD controller doses more insulin when the measured glucose is larger than a target or desired glucose level and less when it is closer to the target (i.e. the proportional part of the controller). The derivative part of an FMPD controller doses more insulin when the measured glucose is rising and less insulin when it is falling. The fading memory aspect of the controller is done by weighting the most recent glucose history more heavily than the more distant glucose values. A detailed description of the OHSU FMPD implementation is given in (Jacobs et al. 2014). The insulin delivery amounts calculated by the control algorithm were sent wirelessly from the phone to the Tandem t:slim pumps. Both pumps receive these data and delivered either insulin or PBS to the participant. In this way, each glucose sensing cannula was delivering an equal volume of either insulin or PBS. Supplemental Figure 4c shows how the OHSU FMPD algorithm was run on the smart phone that communicated with the Dexcom sensor and the Tandem pump. The participants consumed a self-selected meal of 80–150 g of carbohydrate (460 ± 140 calories) at 11am and at 3 PM. Venous blood glucose measurements were taken using a Yellow Springs Instruments (YSI 2300) machine (Toledo, OH) every 15 minutes during the study. Participants were discharged at approximately 6:30 PM.

Quantifying sensor artifact and utilizing smart-sampling

The primary objective of this study was to evaluate whether there was an artifact caused by the delivery of either insulin analog or PBS from the sensing cannula and to quantify the artifact if it was present. Our hypothesis was that there would not be a difference in the artifact of the sensing cannula delivering insulin compared with the sensing cannula delivering PBS. We compared the artifact in the sensor measurement caused by the delivery of the PBS with the artifact caused by the delivery of the insulin. The artifact was quantified as the area under the glucose measurement curve immediately following an insulin or PBS delivery. We calculated the area under the curve (AUC) of the glucose measurement following insulin deliveries and compared the magnitude of the AUC for both insulin vs. PBS boluses. Since the glucose measurement curve has glucose on the y-axis in mmol/L and time in minutes on the x-axis, the units of AUC on this curve is given as mmol/L · min, however we normalized it by the time window over which it was measured, so the final units of AUC are in mmol/L. We evaluated the size of the sensor artifact for large meal boluses for insulin and PBS and compared the size of these artifacts relative to smaller doses that are typical for basal insulin that were given every 5 minutes during the study. For meal boluses, the AUC was measured as the area under the glucose sensing curve from the time that the meal bolus was administered to 30 minutes after the meal bolus. During basal insulin and PBS delivery, the AUC was measured as the area under the glucose sensing curve from the time of the basal delivery to 5 minutes after the delivery.

In addition to quantifying the size of the artifact using the AUC after insulin and PBS deliveries, we also quantified the amount of time required for the sensor to return to within 10% of its baseline value following either a larger *meal bolus* or a smaller *basal delivery*. Because the glucose at baseline is typically changing, it's important to account for the trend

in glucose when calculating the time it takes to return to within 10% of the baseline. Rather than using the baseline glucose itself, we use the baseline glucose projected forward in time based on its trend at the time of the delivery. We first performed a 1-point calibration using the closest preceding YSI measurement to the time that the delivery occurred, to estimate the sensor sensitivity (see Calibration below). Using this estimated sensitivity and the neighboring YSI data points, we projected forward an expected trend line of the sensor over a window of time. We then calculated the settling time, which is the time required for the sensor to return to within 10% of this trend line following a delivery of insulin or PBS. *Smart sampling* is a technique whereby we only include those sensor values which are sampled after the *settling time* that we determined above. Samples acquired after the insulin bolus and before the *settling time* has occurred, are discarded. The purpose of the methods described above was to quantify the size and duration (*settling time*) of the artifact. In real-world usage of smart sampling, calibration would only be required once by the user following the *run-in time* of the sensor. Samples acquired after any meal or basal insulin bolus and before the *settling time* occurred would not be used in the glucose sensor estimations.

Calibration

A secondary objective of the study was to evaluate the accuracy of the sensors using various calibration approaches.

Calibration of a glucose sensor involves converting the sensor's measurements in nano Amperes to a glucose measurement in mmol/L. We used Equation 1 to calibrate the sensor,

$$g(t) = si(t) + b \quad \text{Equation 1}$$

whereby s is the sensitivity of the glucose sensor in units of mmol/L/nA, the background current offset (b) is in mmol/L for zero nA, g(t) is the glucose in mmol/L at a certain time t, and i(t) is the current in nA at that same time t. In our experiments, for a *single-point calibration*, we fixed the background current offset (b) to zero, and then solved for sensitivity, s, using the YSI glucose measured at a single time point, g(t), and the current from the sensor measured at that same time point, i(t), such that the sensitivity is the ratio of the measured glucose and the sensor current, s = g(t)/i(t). The sensitivity is then used to convert future measurements from the sensor in nano Amperes to glucose estimations. The *single-point calibration* is preferred because it requires only one finger-stick for calibration and it represents the way the sensor will typically be used by a person living with diabetes. For an *all-point calibration*, we used each of the YSI measurements taken during the study and the corresponding sensor measurements that matched the YSI glucose in time, and then performed a linear regression to solve for both s and b. For an all-point calibration, s and b are then used to convert sensor current to glucose estimates during the study.

Since YSI measurements were acquired every 15 minutes during the course of the study, we estimated the sensitivity of the sensor to glucose throughout the course of the study. Each study participant wore two sensing cannulae, one delivering insulin and one delivering PBS and each sensing cannula had two sensors, a proximal and a distal sensor. Of the seven participants with usable data, there were a total of 28 sensors to evaluate. When evaluating

the variability of the sensitivity of the sensors during the study, we found that approximately 32% of the sensors (9 out of 28 total sensors) exhibited a material loss of sensitivity during the course of the study as measured by the overall coefficient of variation of sensor sensitivity. This may have been caused by variability in sensing chemistry deposition that led to slower than expected run-in behavior for several of the sensors, with some run-ins extending 4–6 hours, meaning that the sensitivity of the sensors did not settle to a final value until 4–6 hours after the insertion into the body. For this reason, we did two types of analyses, an all-point calibration analysis on all of the data and a single-point calibration analysis on only those sensors (19 out of 28) which did not exhibit the material loss of sensitivity during the course of the study. For the all-point calibration analysis, we evaluated the accuracy of all of the sensors using an *all-point calibration* approach as done by other groups (Lodwig and Heinemann 2003) whereby all YSI glucose readings made throughout the study were used to calibrate the sensing cannula. For this *all-point-calibration*, we solved for s and b in Equation 3 using a linear least squares regression whereby we used matched pairs of YSI for glucose (g) and sensor current measurements (i) in Equation 1. We then used Equation 1 to convert each of the sensor measurements to mmol/L and calculated the mean absolute relative error (MARE) and the mean relative error (MRE) using Equations 2 and 3 below.

$$MARE = \frac{100\%}{N} \sum_{i}^{N} \left| \frac{YSI(i) - sensor(i)}{YSI(i)} \right| \quad \text{Equation 2}$$

$$MRE = \frac{100\%}{N} \sum_{i}^{N} \frac{YSI(i) - sensor(i)}{YSI(i)} \quad \text{Equation 3}$$

While some sensors exhibited a large change in sensitivity during the study, 68% of the sensors did not exhibit this behavior, and these sensors (19 out of 28) were included in the single-point calibration analysis. We show the interquartile range of the sensitivity of each of the 19 sensors that we evaluated in this study in Supplemental Figure 5. Supplemental Figure 5 shows how the sensitivity of the sensors varied throughout the study by calculating the sensitivity of the sensor relative to each YSI measurement using Equation 1. In the single-calibration point analysis evaluated the accuracy for sensors that had a coefficient of variation of sensitivity below 30% during the course of the study (n=19 sensors in 7 participants). For these sensors, we performed a single-point calibration after a 3.5 hour run-in period for the sensors. The 3.5 hour run-in duration was determined based on when the majority of sensors' sensitivity had settled to within a percentage of their final value.

Accuracy of sensors was thereby summarized for (1) all of the sensors using an all-point-calibration and (2) for those 19 sensors with relatively stable sensitivity during the study using a single-point.

Statistical analysis

The mean AUC is calculated by averaging all of the AUC across observations. An AUC may be negative or positive since the sensor reading may go below or above the baseline

trend of glucose, respectively. The mean AUC therefore represents the bias of the artifact. The mean absolute AUC is calculated by averaging the absolute value of the AUC across all observations. The mean absolute AUC therefore represents the magnitude of the artifact without regards to its sign. Mean AUC and mean absolute AUC of glucose following basal and bolus insulin deliveries were estimated using linear regression with the 2×2 factorial design given in Equation 4:

$$Y = \mu + \alpha I + \beta P + \gamma I * P + e, \quad \text{Equation 4}$$

Here, Y represents the mean AUC or mean absolute AUC; I=1 or 0 for observations from the sensing cannula delivering insulin or the sensing cannula delivering PBS, respectively; P=1 or 0 for the proximal or distal sensors; α and β are the coefficients for the main effects, and γ for the interaction. We used bootstrap methods to estimate standard errors (Efron and Tibshirani 1986), taking into account the correlation between each set of four measurements taken in the same time interval on the same person by treating them as clusters. These clusters, rather than individual observations, were sampled with replacement to generate 10,000 bootstrap samples of the same size as the original sample. The linear regression model was fitted to each sample and the standard deviations of the parameter estimates were taken as the standard errors. We evaluated the effects of time since calibration, time since start of analysis, and interpolated YSI separately and together with the sensor characteristics. Because these covariates explained little of the overall variance ($R^2 \leq 0.01$), were not statistically significant, and changed the estimates of the main factors of interest by less than half a percent, we took the more parsimonious model as our main approach.

Means were calculated as linear combinations of the regression coefficients: μ, μ+α, μ+β, and μ+α+β+γ represent the means for the sensor for the distal sensing electrode on the cannula delivering PBS, the distal sensing electrode on the cannula delivering insulin, the proximal sensing electrode on the cannula delivering PBS, and the proximal sensing electrode on the cannula delivering insulin, respectively. In addition to the four cell means, we were interested in the average differences between proximal vs. distal sensors, and between sensors on cannulae delivering insulin vs. PBS. We calculated these average differences using similar linear combinations and used two-sided Wald tests to calculate P-values. We performed this analysis independently for both the basal insulin deliveries and for the bolus deliveries. We additionally performed an independent two-tailed t-test comparing recovery time for large boluses and basal deliveries. We considered a P-value of less than 0.05 to indicate statistical significance. Stata/IC version 15 (StataCorp, College Station TX) was used for regression analyses.

Results

Impact of Insulin and PBS on Measurement Artifact

We found that both the PBS infusion and the insulin infusion caused an artifact (Figure 2).

Notice in Figure 2 (row 1) that the glucose tends to trend upward over the observation window after a meal bolus as indicated by the rising YSI and sensor measurements. There

is no increasing trend following basal insulin delivery as these smaller boluses were not synchronous with meals (row 2 of Figure 2).

Figure 2 shows that the current on average decreased following the larger meal boluses while the same type of decrease is not apparent for smaller basal deliveries even though statistically, the artifact was present for both basal and bolus deliveries. The recovery time (Figure 3) was also longer for the larger boluses (10.3 ± 8.5 minutes) than for the smaller basal deliveries (41.2 ± 78.3 seconds, $P<0.05$).

Tables 1a and 1b show the estimated means of AUC and the absolute value of AUC, respectively, for insulin proximal, insulin distal, PBS proximal, and PBS distal sensors, along with bootstrapped standard errors clustered in five-minute intervals. The AUC values had a symmetric, non-normal distribution with a wide range (±135, approximately) but with more than 80% of values falling between ±10. The mean AUCs were generally small (<0.435 mmol/L) and not statistically different from zero for any of the basal insulin deliveries or distal meal bolus deliveries. However, the mean AUCs were significantly less than zero, on average, for proximal insulin and PBS bolus deliveries (−0.772 and −1.004 mmol/L, respectively). On the absolute scale, all AUCs differed significantly from zero. Basal absolute AUCs ranged from 0.22 to 0.5 mmol/L, with distal deliveries measuring higher than proximal, and insulin delivering sensing cannulae higher than PBS delivering cannulae.

Contrasting insulin vs. PBS and proximal vs. distal

Table 2 shows the mean differences in sensing cannula artifacts for insulin vs. PBS and for distal vs. the proximal sensors.

The mean AUC and mean absolute AUC are significantly different when insulin is delivered compared with PBS for basal insulin and basal PBS deliveries, however the differences are less than 0.10 mmol/L. For larger insulin and PBS boluses, sensing cannulae that were delivering insulin were not significantly different than those delivering PBS. There was a significant difference in mean absolute AUC between proximal vs. distal sensors for basal deliveries ($P<0.001$) and a trending toward significant difference in mean AUC between proximal vs. distal sensors, whereby the proximal sensor had a larger negative artifact than the distal sensor (−0.172 mmol/L, $P=0.07$) 0.172 mmol/L or less. If a person’s glucose was 5.5 mmol/L, this would represent an error of 3% caused by the insulin compared with the PBS, which is still substantially lower than the typical error observed in CGM systems. There was not a significant difference in either mean AUC or mean absolute AUC for proximal vs. distal bolus deliveries (Supplemental Figure 2).

Accuracy results

When all sensors were considered, an all-point calibration resulted in a MARE of 9.5 ± 4.5% and an MRE of −1.6 ± 1.5%.

There was a benefit of using the Kalman filter smoothing algorithm and the smart sampling. This benefit is captured in Table 3 which shows how use of the Kalman filter smoothing algorithm helped reduce the MARE from 10.9% to 9.5% for the all-point calibration (all

sensors) and from 17.3% to 14.0% for the single-point calibration (selected sensors with sensitivity coefficient of variation<30%).

Clarke error grids showing the predicted vs. actual glucose sensor data are shown in Supplemental Figure 3 for the all-point-calibration and the single-point calibration of those sensors that had low sensitivity coefficient of variation (<30%). Notice that 96.7 % of the data was in the A and B regions of the charts for the all-calibration analysis and 97.5% for the single-point calibration analysis.

Discussion

In this paper, we have shown that in adults with T1D, when a redox-mediated glucose sensing cannula is biased at a low voltage potential (175 mV), there remains an artifact imposed on the sensor that is likely due to dilution around the sensing element. We have shown that this artifact is likely not caused by the preservatives within insulin formulations (meta cresol and phenol) as has been observed using conventional sensors in vitro and in vivo (Ward et al. 2017). We believe that this artifact is caused at least in part by dilution of glucose in the vicinity of the sensor, rather than as a result of interaction with m-cresol or phenol because the artifact was present in both the sensing cannulae delivering insulin and the sensing cannulae delivering PBS. The absolute value of the artifact was found to be slightly larger for the sensing elements located distal (i.e. closer to the point of fluid delivery) compared with proximal for basal delivery amounts, again indicating that the fluid was diluting the area around the sensor elements and impacting the proximal sensor less substantially. However, the difference in the distal vs. proximal sensors for basal delivery amounts was small at less than 0.172 mmol/L. This amount of error is considered small because it equates to a relatively small error that is substantially less than the error typically observed in a CGM. For example, if the CGM reading was 5.5 mmol/L, the difference in the proximal vs. distal sensor would represent only a 3% difference, which is well below the typical CGM error of 9% in state-of-the-art CGM systems. The bolus artifact was substantially larger for meal bolus delivery amounts as shown in Table 1, where the artifact size ranged from 1.085 to 1.32 mmol/L. If the person’s CGM was measured to be 5.5 mmol/L, the error introduced by the meal bolus artifact would potentially introduce nearly 24% of error on the sensor. These results indicate that care must be taken with the design of sensing cannulae to (1) be selective about where the sensing element is placed relative to the point of delivery of insulin for sensing cannulae designed for AID systems and (2) practice smart sampling to avoid incorporating sensor values into the measurement when an artifact is known to be present.

In Ward et al. (2017) it was shown in-vitro that when a conventional platinum-based, peroxide-measuring glucose sensor (biased at 500–700 mV) is exposed to specific insulin excipients (phenol and/or m-cresol) there is a very large initial oxidation spike artifact as the phenolic is oxidized. Then, over a period of minutes to hours, there is an electropolymerization of the phenolics which forms a polymer layer on the electrode. This layer permanently poisons the electrode, and as it forms, the current progressively decays to low levels. In contrast, an osmium redox mediator-based sensor with a gold indicating electrode, biased at 175–180 mV undergoes no change (no initial oxidation spike and no

progressive loss of current) when exposed to phenolic excipients. In vitro experiments verified that the phenol and cresol do not oxidize at these lower bias potentials. The results presented in this paper demonstrate that while there is still an artifact caused by the delivery of insulin in close proximity to the glucose sensing element, the artifact is nearly identical to the artifact caused by the delivery of PBS. This implies that the interference of the m-cresol and phenols within the insulin are not causing the artifact *per se*.

In the sensing cannula design presented in this paper, the distal sensor was 4.6 mm from the tip (point of fluid delivery) while the proximal sensor element was 6.3 mm from the tip. The results found in this paper do not conflict with the findings from other groups including Hermanides' (2008), Linde and Philip (1989), and O'Neal et al. (2013), all of whom had inserted the sensors at least 7 mm away from the point of insulin delivery and found no artifact. We believe that the reason that they did not see an artifact is because the distance between the sensor and the insulin delivery port were far enough away to avoid such an artifact. Our human results are also in agreement with the swine study of Rodriguez et al. (2011) who showed that for the sensor placed 5 mm from the port of insulin delivery, there was a statistically significant difference from a sensor that was far away (10–15 cm).

We have also shown in this paper a method for doing smart sampling and data smoothing to further reduce the artifact caused by insulin delivery. Results indicate that smart sampling and use of the Kalman data smoother algorithm presented in this paper improved the accuracy from 10.9% to 9.5% for the all-point-calibration and from 17.3% to 14.0% for the single-point calibration result.

There were several limitations of this study. First, there was a small number of study participants (n=7) included in this data analysis. Despite these small numbers, we were able to show that there is a statistically significant difference in the proximal vs. distal sensors caused by the dilution artifact for basal insulin deliveries. While the number of participants is small, we have a large number of observations of the artifact for basal deliveries (n=2096) and meal bolus deliveries (n=60) of both insulin and PBS solution. The large numbers of observations have enabled us to quantify the size and duration of the artifact. Our statistical analysis did not determine that there was a participant-specific effect (from the mixed effects analysis), thereby indicating that the artifact estimates were generally consistent across each of the participants and not being dominated by differences amongst the participants. Second, the duration of the study was relatively short. Because the sensors required 3.5 hours to run-in, the average time over which the sensing cannulae were evaluated was 4.8 ± 0.5 hours. In the future, we are planning a longer 7-day study to evaluate the performance of this sensing cannula. Another limitation was that some of the sensors exhibited lengthy run-ins that resulted in a high coefficient of variation in sensor sensitivity during the study, which made it challenging to analyze the accuracy on all sensors without doing an all-point calibration. In this early version of the biosensor, a manufacturing method had not yet been created and for this reason, there were many manual steps which introduced a great deal of variability in terms of outer membrane thickness, outer membrane pinholes, enzyme-redox mediator-polymer deposition amounts, and variability in the adhesion of all layers to one another. We believe that these variabilities and suboptimal adhesion caused sensor instability (changes in sensitivity over time). For the single-point calibration analysis, we elected to

confine the analysis to the 19 sensors that did not undergo more than a 30% change in sensitivity over time. Currently, PDT is working on creating a more reproducible sensor manufacturing system. We have implemented several key design changes to the sensor chemistry that will substantially reduce the run-in time and also reduce the variability of sensor sensitivity that we observed in this study. In our future studies, we plan to explore the effectiveness of these design changes in the performance of the glucose sensing cannula.

Conclusions

We have provided methods for measuring glucose with reasonable accuracy using a redox-mediated sensor mounted directly on an insulin infusion cannula in humans with type 1 diabetes. After bolus deliveries, there are short-lived artifacts, likely caused by dilution around the sensing element, that are proportional to the volume of the bolus and are similar in magnitude for insulin vs PBS delivery. The magnitude of such artifacts is related to the proximity of the electrode to the site of fluid delivery for basal deliveries, however the difference between the proximal and distal sensor readings is small at less than 0.167 mmol/L. We conclude that using a redox mediator-based sensing chemistry biased at +175 mV, artifacts from insulin preservatives are not observed, since the artifact from insulin delivery was nearly identical to the artifact from PBS delivery. We also provide a method for data filtering and selective temporal sampling to reduce error by accounting for delays between interstitium and plasma and by excluding data points immediately following a bolus of insulin.

Supplementary Material

Refer to Web version on PubMed Central for supplementary material.

Acknowledgements

The guarantor of this research is Peter G. Jacobs who takes responsibility for the contents of the article. This work was supported by grants from the National Institutes of Health (grant 1DP3DK101044, 1R43DK096678, 1R43DK100996, and 1R43DK109806), the Leona M. and Harry B. Helmsley Charitable Trust (2015PG-T1D046), and by Oregon Clinical and Translational Research Institute UL1TR002369 from the National Center for Advancing Translational Sciences at the NIH. Conflicts of Interest: PGJ, TS, RC, WKW, SV, KM, SB and JRC have a financial interest in Pacific Diabetes Technologies Inc., a company that may have a commercial interest in the results of this research and technology. CML and NT report no conflicts of interest. We wish to thank Tomas Walker (Dexcom) and Vance Swanson (Tandem) for their support of the study. We wish to thank Matthew Breen, Brennen McCullough, Chad Knutsen, and Scott Campbell for their help to fabricate the devices.

References

Castle JR, El Youssef J, Wilson LM, Reddy R, Resalat N, Branigan D, Ramsey K, Leitschuh J, Rajhbeharrysingh U, Senf B, Sugerman SM, Gabo V, Jacobs PG, 2018. Randomized Outpatient Trial of Single- and Dual-Hormone Closed-Loop Systems That Adapt to Exercise Using Wearable Sensors. Diabetes Care 41(7), 1471–1477. [PubMed: 29752345]

Clarke WL, Cox D, Gonder-Frederick LA, Carter W, Pohl SL, 1987. Evaluating clinical accuracy of systems for self-monitoring of blood glucose. Diabetes Care 10(5), 622–628. [PubMed: 3677983]

Efron B, Tibshirani R, 1986. Bootstrap Methods for Standard Errors, Confidence Intervals, and Other Measures of Statistical Accuracy. Statist. Sci. 1(1), 54–75.

Foster NC, Beck RW, Miller KM, Clements MA, Rickels MR, DiMeglio LA, Maahs DM, Tamborlane WV, Bergenstal R, Smith E, Olson BA, Garg SK, 2019. State of Type 1 Diabetes Management and

Outcomes from the T1D Exchange in 2016–2018. Diabetes Technol. Ther. 21(2), 66–72. [PubMed: 30657336]

Foster NC, Miller KM, Tamborlane WV, Bergenstal RM, Beck RW, Network TDEC, 2016. Continuous Glucose Monitoring in Patients With Type 1 Diabetes Using Insulin Injections. Diabetes Care 39(6), e81–e82. [PubMed: 27208319]

Hermanides J, Wentholt IM, Hart AA, Hoekstra JB, DeVries JH, 2008. No Apparent Local Effect of Insulin on Microdialysis Continuous Glucose- Monitoring Measurements. Diabetes Care 31(6), 1120–1122. [PubMed: 18332157]

Hovorka R, Kumareswaran K, Harris J, Allen J, Elleri D, Xing D, Kollman C, Nodale M, Murphy H, Dunger D, Amiel S, Heller S, Wilinska M, Evans M, 2011. Overnight closed loop insulin delivery (artificial pancreas) in adults with type 1 diabetes: crossover randomised controlled studies. BMJ 342(1855).

Jacobs PG, El Youssef J, Castle J, Bakhtiani P, Branigan D, Breen M, Bauer D, Preiser N, Leonard G, Stonex T, Ward WK, 2014. Automated control of an adaptive bihormonal, dual-sensor artificial pancreas and evaluation during inpatient studies. IEEE Trans Biomed Eng 61(10), 2569–2581. [PubMed: 24835122]

Jacobs PG, El Youssef J, Reddy R, Resalat N, Branigan D, Condon J, Preiser N, Ramsey K, Jones M, Edwards C, Kuehl K, Leitschuh J, Rajhbeharrysingh U, Castle JR, 2016. Randomized trial of a dual-hormone artificial pancreas with dosing adjustment during exercise compared with no adjustment and sensor-augmented pump therapy. Diabetes Obes Metab 18(11), 1110–1119. [PubMed: 27333970]

Jacobs PG, Resalat N, El Youssef J, Reddy R, Branigan D, Preiser N, Condon J, Castle J, 2015. Incorporating an Exercise Detection, Grading, and Hormone Dosing Algorithm Into the Artificial Pancreas Using Accelerometry and Heart Rate J Diabetes Sci Technol 9(6), 1175–1184. [PubMed: 26438720]

Kropff J, Del Favero S, Place J, Toffanin C, Visentin R, Monaro M, Messori M, Di Palma F, Lanzola G, Farret A, Boscari F, Galasso S, Magni P, Avogaro A, Keith-Hynes P, Kovatchev BP, Bruttomesso D, Cobelli C, DeVries JH, Renard E, Magni L, 2015. 2 month evening and night closed-loop glucose control in patients with type 1 diabetes under free-living conditions: a randomised crossover trial. Lancet Diabetes Endocrinol 3(12), 939–947. [PubMed: 26432775]

Linde B, Philip A, 1989. Massage-enhanced insulin absorption--increased distribution or dissociation of insulin? Diabetes Res 11(4), 191–194. [PubMed: 2696618]

Lindpointner S, Korsatko S, Kohler G, Kohler H, Schaller R, Kaidar R, Yodfat O, Schaupp L, Ellmerer M, Pieber TR, Regittnig W, 2010. Use of the site of subcutaneous insulin administration for the measurement of glucose in patients with type 1 diabetes. Diabetes Care 33(3), 595–601. [PubMed: 20040654]

Lodwig V, Heinemann L, 2003. Continuous glucose monitoring with glucose sensors: calibration and assessment criteria. Diabetes Technol Ther 5(4), 572–586. [PubMed: 14511412]

Nacht B, Larndorfer C, Sax S, Borisov SM, Hajnsek M, Sinner F, List-Kratochvil EJ, Klimant I, 2015. Integrated catheter system for continuous glucose measurement and simultaneous insulin infusion. Biosens Bioelectron 64, 102–110. [PubMed: 25194803]

O'Neal DN, Adhya S, Jenkins A, Ward G, Welsh JB, Voskanyan G, 2013. Feasibility of adjacent insulin infusion and continuous glucose monitoring via the Medtronic Combo-Set. Journal of Diabetes Science and Technology 7(2), 381–388. [PubMed: 23566996]

Peters T, Haidar A, 2018. Dual-hormone artificial pancreas: benefits and limitations compared with single-hormone systems. Diabet. Med. 35, 450–459. [PubMed: 29337384]

Regittnig W, Lindpointner S, Korsatko S, Tutkur D, Bodenlenz M, Pieber TR, 2013. Periodic extraction of interstitial fluid from the site of subcutaneous insulin infusion for the measurement of glucose: a novel single-port technique for the treatment of type 1 diabetes patients. Diabetes Technol Ther 15(1), 50–59. [PubMed: 23126579]

Renard E, Farret A, Kropff J, Bruttomesso D, Messori M, Place J, Visentin R, Calore R, Toffanin C, Di Palma F, Lanzola G, Magni P, Boscari F, Galasso S, Avogaro A, Keith-Hynes P, Kovatchev B, Del Favero S, Cobelli C, Magni L, JH D, 2016. Day-and-Night Closed-Loop Glucose Control in Patients With Type 1 Diabetes Under Free-Living Conditions: Results of a Single-Arm 1-Month

Experience Compared With a Previously Reported Feasibility Study of Evening and Night at Home. Diabetes Care 39(7), 1151–1160. [PubMed: 27208331]

Rodriguez LT, Friedman KA, Coffman SS, Heller A, 2011. Effect of the sensor site-insulin injection site distance on the dynamics of local glycemia in the minipig model. Diabetes Technol Ther 13(4), 489–493. [PubMed: 21355724]

Russell SJ, El-Khatib FH, Sinha M, Magyar KL, McKeon K, Goergen LG, Balliro C, Hillard MA, Nathan DM, Damiano ER, 2014. Outpatient glycemic control with a bionic pancreas in type 1 diabetes. N Engl J Med 371(4), 313–325. [PubMed: 24931572]

Smalley E, 2016. Medtronic automated insulin delivery device gets FDA nod. Nat Biotechnol 34(12), 1220. [PubMed: 27926704]

Thabit H, Lubina-Solomon A, Stadler M, Leelarathna L, Walkinshaw E, Pernet A, Allen JM, Iqbal A, Choudhary P, Kumareswaran K, Nodale M, Nisbet C, Wilinska ME, Barnard KD, Dunger DB, Heller SR, Amiel SA, Evans ML, Hovorka R, 2014. Home use of closed-loop insulin delivery for overnight glucose control in adults with type 1 diabetes: a 4-week, multicentre, randomised crossover study. Lancet Diabetes Endocrinol 2(9), 701–709. [PubMed: 24943065]

Ward WK, Heinrich G, Breen M, Benware S, Vollum N, Morris K, Knutsen C, Kowalski JD, Campbell S, Biehler J, Vreeke MS, Vanderwerf SM, Castle JR, Cargill RS, 2017. An Amperometric Glucose Sensor Integrated into an Insulin Delivery Cannula: In Vitro and In Vivo Evaluation. Diabetes Technol Ther 19(4), 226–236. [PubMed: 28221814]

Weisman A, Bai JW, Cardinez M, Kramer CK, Perkins BA, 2017. Effect of artificial pancreas systems on glycaemic control in patients with type 1 diabetes: a systematic review and meta-analysis of outpatient randomised controlled trials. Lancet Diabetes Endocrinol 5(7), 501–512. [PubMed: 28533136]

Highlights

- A redox-mediated glucose sensor mounted on an insulin infusion cannula was fabricated and tested in people with type 1 diabetes during an automated insulin and saline infusion study.
- Infusing insulin or saline through a redox-mediated glucose sensor can cause a small dilution artifact which increases in size for larger infusions.
- Polarizing a glucose sensor located at the site of insulin infusion at a voltage potential of 175 mV can reduce sensor artifacts caused by insulin excipients such that the artifact is nearly the same as a dilution artifact caused by saline solution.
- Strategic sampling and signal processing methods including Kalman filtering can reduce error from dilution artifacts

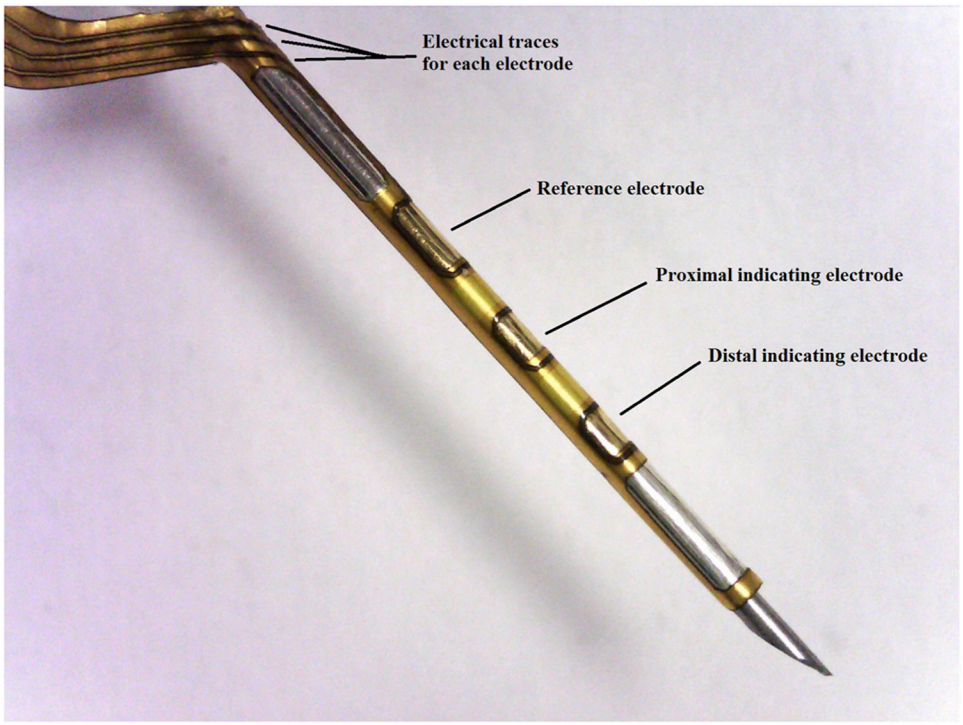

Figure 1:
The Pacific Diabetes Technologies glucose-sensing cannula.

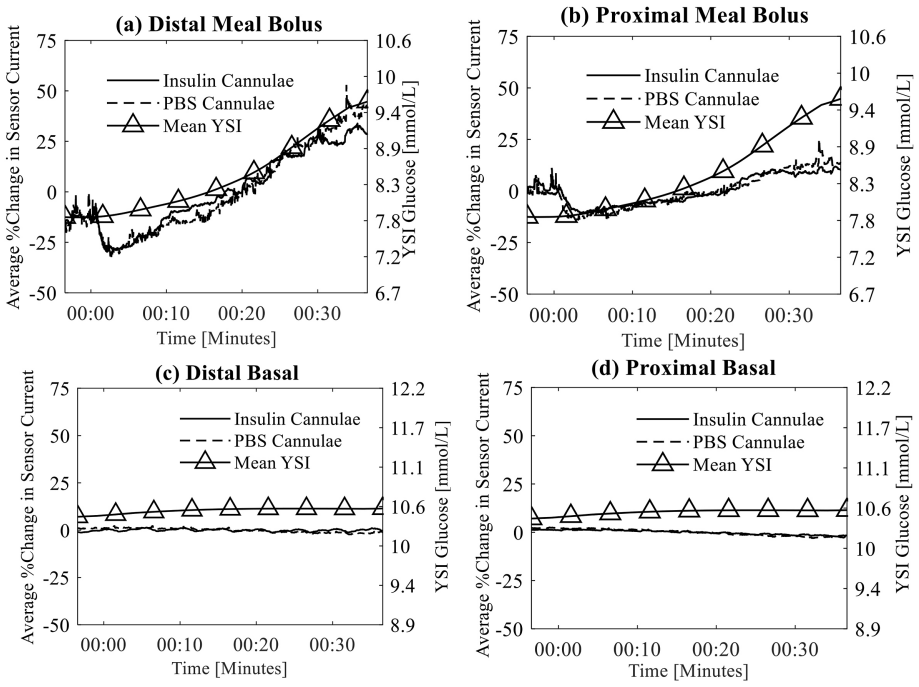

Figure 2:

Top row shows the mean artifact of sensors from cannulae that are delivering insulin and PBS meal bolus amounts as measured by the distal (a) and proximal (b) sensing cannulae. The fluid delivery occurs at time 00:00. Bottom row shows mean artifact of sensors from cannulae that are delivering insulin and PBS basal amounts as measured by distal (c) and proximal (d) sensing cannulae. Blood glucose as measured by the YSI is also shown in each of these plots using the right y-axis. Notice that the sensors on the cannuae delivering insulin are nearly identical to those delilvery PBS and therefore a difference between those lines is not apparent.

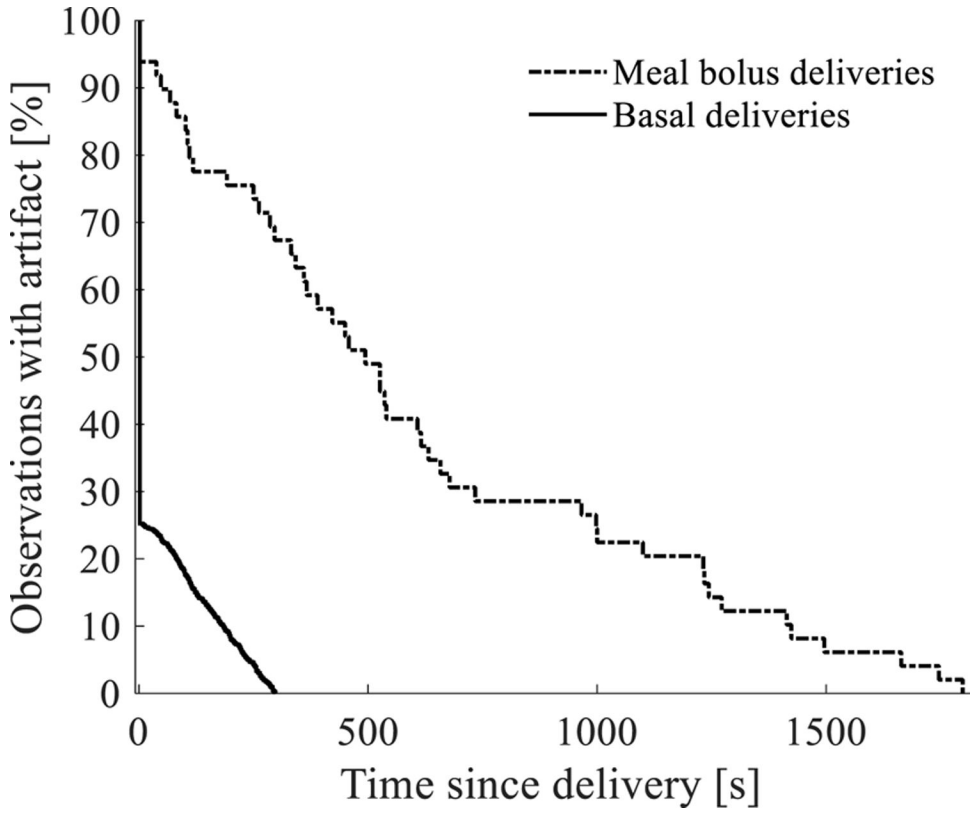

Figure 3:

Survival curve showing the percentage of observations after fluid delivery (insulin or PBS solution) that are free of the artifact vs. the time since the fluid was delivered. Immediately after fluid is delivered, most sensor observations exhibit some form of artifact, but the artifact is not present as time passes. Sensor recovery time is shown to be dependent on bolus volume whereby 70–80% of the smaller basal deliveries are free of artifact after 100 seconds while 70–80% of the sensor observations are free of artifact after 10 minutes for larger meal boluses.

Table 1:

Mean AUC (a) and mean absolute AUC (b) for basal and bolus insulin deliveries. Results show the mean AUC across the different sensor conditions (insulin distal, insulin proximal, PBS distal, and PBS proximal). The mean, standard error (SE), and 95% confidence intervals (CIs) are for the AUC under each sensor condition and were calculated using linear regression with bootstrapping clustered on the four sensor conditions measured at the same time point. The P-values reflect statistical significance for the test that the mean differs from 0. (N=7 participants, 524 basal clusters [2,096 observations], and 12 bolus clusters [60 observations]).

(a) Mean AUC						
		Mean [mmol/L]	**SE [mmol/L]**	**P-value**	**95% CI Lower [mmol/L]**	**95% CI Upper [mmol/L]**
Basal	**Insulin, distal**	0.071	0.038	0.06	−0.002	0.145
	Insulin, proximal	0.010	0.026	0.7	−0.041	0.061
	PBS distal	−0.008	0.034	0.81	−0.075	0.058
	PBS proximal	−0.034	0.020	0.08	−0.073	0.004
Bolus	**Insulin distal**	−0.416	0.331	0.21	−1.065	0.233
	Insulin proximal	−0.772	0.295	0.01	−1.351	−0.193
	PBS distal	−0.435	0.432	0.31	−1.282	0.413
	PBS proximal	−1.004	0.178	<0.001	−1.353	−0.656
(b) Mean absolute AUC						
		Mean [mmol/L]	**SE [mmol/L]**	**P-value**	**95% CI Lower [mmol/L]**	**95% CI Upper [mmol/L]**
Basal	**Insulin distal**	0.497	0.032	<0.001	0.435	0.559
	Insulin proximal	0.329	0.021	<0.001	0.287	0.371
	PBS distal	0.420	0.029	<0.001	0.364	0.477
	PBS proximal	0.245	0.017	<0.001	0.212	0.277
Bolus	**Insulin distal**	1.085	0.208	<0.001	0.678	1.492
	Insulin proximal	1.175	0.187	<0.001	0.809	1.541
	PBS distal	1.320	0.295	<0.001	0.742	1.899
	PBS proximal	1.022	0.173	<0.001	0.683	1.361

Table 2:

Mean differences for insulin vs. PBS and proximal vs. distal sensors in (a) mean AUC and (b) mean absolute AUC.

(a) Differences in mean AUC						
		Mean [mmol/L]	**SE [mmol/L]**	**P-value**	**95% CI Lower [mmol/L]**	**95% CI Upper [mmol/L]**
Basal	**Insulin vs. PBS**	0.062	0.031	0.04	0.002	0.122
	Proximal vs. distal	−0.044	0.024	0.07	−0.091	0.003
Bolus	**Insulin vs. PBS**	0.126	0.331	0.7	−0.524	0.775
	Proximal vs. distal	−0.463	0.343	0.18	−1.135	0.209
(b) Differences in mean absolute AUC						
		Mean [mmol/L]	**SE [mmol/L]**	**P-value**	**95% CI Lower [mmol/L]**	**95% CI Upper [mmol/L]**
Basal	**Insulin vs. PBS**	0.081	0.027	0.003	0.027	0.133
	Proximal vs. distal	−0.172	0.020	<0.001	−0.211	−0.132
Bolus	**Insulin vs. PBS**	−0.042	0.217	0.85	−0.468	0.385
	Proximal vs. distal	−0.104	0.189	0.58	−0.474	0.267

Table 3:

MARE of glucose sensing cannula using various signal processing methods.

	Error with no signal processing [%]	**Error with linear regression smoothing [%]**	**Error with two-stage Kalman smoother + smart sampling [%]**
All sensors (all-point calibration)	10.9 ± 4.6	10.9 ± 4.5	9.5 ± 4.5
Select sensors (single-point calibration)	17.3 ± 8.5	16.5 ± 7.2	14.0 ± 5.9